NANO LETTERS

Letter

pubs.acs.org/NanoLett

Harmonic Oscillator Wave Functions of a Self-Assembled InAs Quantum Dot Measured by Scanning Tunneling Microscopy

Karen Teichmann,[†] Martin Wenderoth,*[,†] Henning Prüser,[†] Klaus Pierz,[‡] Hans W. Schumacher,[‡] and Rainer G. Ulbrich[†]

[†]IV. Physikalisches Institut, University of Göttingen, Friedrich-Hund-Platz 1, 37077 Göttingen, Germany

[‡]Physikalisch-Technische Bundesanstalt, Bundesallee 100, 38116 Braunschweig, Germany

ABSTRACT: InAs quantum dots embedded in an AlAs matrix inside a double barrier resonant tunneling diode are investigated by cross-sectional scanning tunneling spectroscopy. The wave functions of the bound quantum dot states are spatially and energetically resolved. These bound states are known to be responsible for resonant tunneling phenomena in such quantum dot diodes. The wave functions reveal a textbook-like one-dimensional harmonic oscillator behavior showing up to five equidistant energy levels of 80 meV spacing. The derived effective oscillator mass of $m^* = 0.24m_0$ is 1 order of magnitude higher than the effective electron mass of bulk InAs that we attribute to the influence of the surrounding AlAs matrix. This underlines the importance of the matrix material for tailored QD devices with well-defined properties.

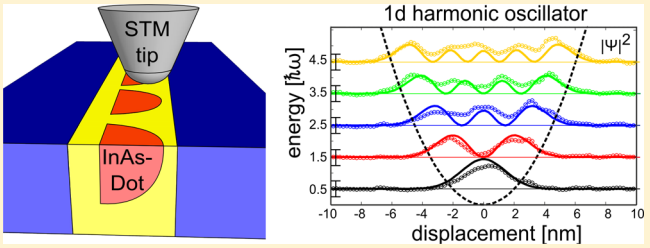

KEYWORDS: *Self-assembled quantum dots, STM, STS, harmonic oscillator, III−V semiconductor*

InAs self-assembled quantum dots (QD) have been in the focus of a wide range of scientific studies for almost two decades. These investigations have been driven both by potential applications as well as by fundamental questions (see as review, e.g., ref 1). The optical and electrical properties of the InAs QDs, and hence their potential for applications, strongly depend on the spatial structure of the wave functions of the bound QD states. For InAs QDs on the surface of a GaAs substrate, the wave functions have been spatially imaged and energetically resolved using scanning tunneling spectroscopy (STS) in ultrahigh vacuum (UHV).[2] However, in functional device structures the QDs are usually embedded in a semiconductor matrix by overgrowth of epitaxial capping layers. One way to access the spatial distribution of the wave function of such embedded QDs is by magneto-tunneling spectroscopy[3,4] or magneto-capacitance spectroscopy[5] in combination with suitable theoretical modeling.[6] Also cross-sectional scanning tunneling microscopy (STM) and STS on cleaved surfaces can be used to access the geometry and bound state wave functions of the QDs. The topography, shape, and composition of InAs QDs in a GaAs matrix[7,8] have been studied, as well as the laterally resolved QD wave functions by STS[9−11] and by local $I(V)$-spectroscopy.[12] Recently, similar experiments have also been carried out on self-assembled InAsP QDs embedded in InP.[13,14] This material system forms rather large QDs resulting in a complex energy structure of the QD bound states superimposed from quantization in lateral and growth direction.

For certain applications such as resonant tunneling diodes it has proven useful to embed InAs QDs in a different matrix material than GaAs, for example, in a large band gap AlAs tunnel barrier layer.[15] In such devices, the change of the matrix material should modify the bound QD states resulting in a different energy spectrum and a different spatial wave function structure of the QD. However, spatially resolved imaging and spectroscopy of InAs QD wave functions in a different matrix material than GaAs have not been reported, yet.

In this letter we study self-assembled InAs quantum dots embedded in an AlAs matrix by STM and STS on a cleaved cross sectional surface in UHV. The smaller dimensions of these InAs QDs grown on AlAs compared to InAs QDs grown on GaAs[16] as well as the higher confinement potential of AlAs compared to GaAs result in a stronger quantum confinement of electrons and holes in this system. The spatially and energetically resolved QD states reveal a textbook-like one-dimensional harmonic oscillator behavior. Up to five equidistant energy levels of 80 meV spacing are observed. The effective electron mass of the harmonic oscillator model $m^* = 0.24m_0$ is about an order of magnitude larger than the effective mass in bulk InAs. We attributed this to the influence of the surrounding AlAs matrix.

The experiments are performed in a custom built low temperature STM working under UHV conditions ($<1 \times 10^{-11}$ mbar). The tips are electrochemically etched from a polycrystalline tungsten wire. The differential conductivity dI/dV signal is derived numerically from the I/V spectroscopy measurement.[17] In transport measurements, the sample has shown the typical characteristics of a resonant tunneling

Received: April 4, 2013
Revised: June 13, 2013
Published: June 18, 2013

   dx.doi.org/10.1021/nl401217q | *Nano Lett.* 2013, 13, 3571−3575

diode.[15] It is grown by molecular-beam epitaxy (MBE) on a silicon-doped (N_D ~2 × 10^{18} cm^{-3}) GaAs(001) substrate. The structure consists of an undoped GaAs prelayer of 15 nm followed by a 6 nm AlAs barrier. On that barrier, 1.8 monolayers of InAs are deposited and self-assembled InAs quantum dots are formed by Stranski–Krastanov growth on a monatomic InAs wetting layer. The structure is continued by a 6 nm AlAs barrier and an undoped 15 nm GaAs layer on top. More details of the sample and the growth process can be found in ref 15. The samples are cleaved under UHV condition and the $(\bar{1}10)$ surface that is perpendicular to the growth direction is investigated. The sample system including the STM tip is schematically sketched in Figure 1.

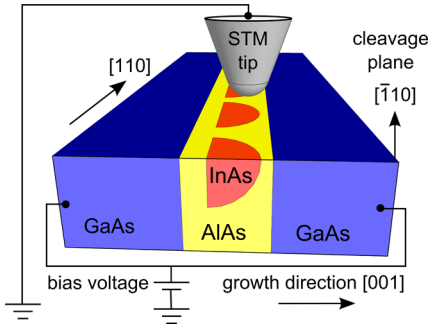

Figure 1. Sketch of the sample system and STM setup. InAs quantum dots (red) are grown between two 6 nm wide AlAs barriers (yellow) embedded inside GaAs (blue). The sample is cleaved perpendicular to the heterostructure in the $(\bar{1}10)$ crystal plane, and the cleaved quantum dots can be investigated by the STM-tip.

In the following, the local density of states of a single quantum dot are experimentally characterized and compared to the solutions of the one-dimensional quantum-mechanical harmonic oscillator. The most important characteristic of the harmonic oscillator solution of the Schrödinger equation is that the discrete energy eigenstates are equally spaced. A second characteristic that can be tested is that the number of antinodes of the wave functions increases by one for each higher energy level, starting with one antinode for the wave function with the lowest energy. The spatial extension of the wave functions increases as well, which is expected for the solutions of the harmonic potential.

A constant current topography image (27 × 27 nm^2) of the cleaved InAs QD is shown in Figure 2a. The bright spots show the distribution of InAs that is embedded in the 6 nm AlAs layer below and above (dark areas). The QD displays a lens shape with a base width of ~15 nm and a height of ~3 nm sitting on the InAs wetting layer along the (001) plane. Although the exact position of the cleavage plane is not known, we estimate from comparison with transmission electron microscopy (TEM) images[16] that the QD is cut close to the center diameter and the remaining InAs extends to a depth of about 7 nm or less along the $[1\bar{1}0]$ direction into the AlAs substrate.

The green box in Figure 2a indicates the area (16 × 16 nm^2) where the spatially resolved differential conductivity ($dI/dV(x,y)$) is recorded, which is a measure of the energy resolved local density of stated (LDOS). The $dI/dV(x,y)$-maps are shown in Figure 2b–f for different bias voltages of (b) 0.69, (c) 0.80, (d) 0.91, (e) 1.01, and (f) 1.10 V. They display the spatial distribution of the electron density, that is, the squared

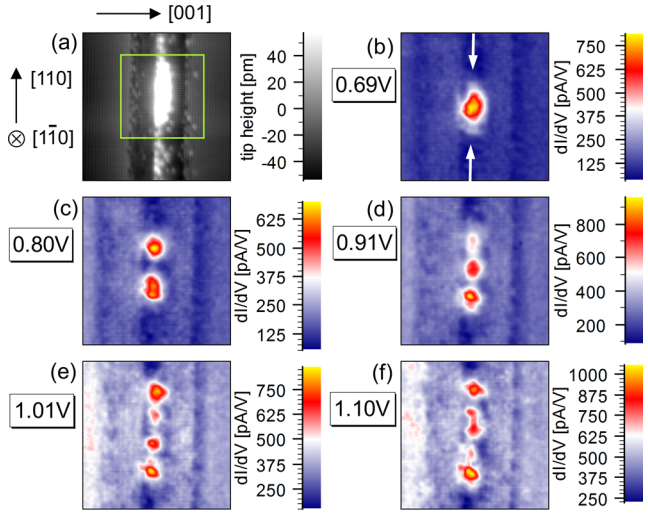

Figure 2. (a) A constant current topography image (27 × 27 nm^2) taken at a bias voltage of +2 V and a current of 0.9 nA of the investigated InAs quantum dot. The green box in (a) shows the area (16 × 16 nm^2) where the differential conductivity $dI/dV(x,y)$-maps are taken. (b–f) Spatially resolved $dI/dV(x,y)$-maps for different bias voltages. In each image, the number of peaks of the wave function is increased by one and the bias voltage is almost equally spaced.

electronic wave functions $|\Psi(x,y)|^2$. With increasing bias voltage at a value of 0.69 V (Figure 2b), a first dI/dV signal peak is observed nearly in the center of the InAs quantum dot which can be attributed to the ground-state wave function. With increasing bias voltage, the signal disappears until at about 0.80 V (Figure 2c) two well pronounced peaks appear, slightly shifted to the edges of the QD. These two signals are attributed to the wave functions of the first excited state. Three separated signals are observed when the bias voltage is again increased by about 0.1 to a value of 0.91 V (Figure 2d) that are associated with the wave functions of the second excited state. For this level, one signal is located in the center and the other ones are shifted to the edges of the QD. With increasing bias voltage steps of about 0.1 to higher bias voltage values of 1.01 and of 1.1 V, four and five dI/dV peaks are observed, respectively, which are attributed to the next higher quantum numbers of an harmonic oscillator. These measurements clearly show that at least five electron energy levels can be resolved in the QD. The number of antinodes increases by one per level with an equidistant bias voltage spacing of approximately 0.1 V.

The observed characteristics of the InAs QD wave functions thus agree very well with the above-described characteristics of a 1D quantum-mechanical harmonic oscillator. These similarities become clearer if one visualizes the wave functions both resolved spatially and energetically. This is shown in Figure 3, where a $dI/dV(x,V)$-section along a line indicated by the arrows in Figure 2b is displayed. The number of antinodes of the wave function increases by one for each higher electron level n, starting with one antinode for the wave function n = 0 with the lowest energy. For the even levels n = 0, 2, and 4 one antinode is always located in the center of the harmonic oscillator (around x = 0 nm in Figure 3), whereas for the uneven levels no antinode is found, here. With increasing n, the positions of the outer antinodes of the wave function move away from the center along $\pm x$. Such increase of the spatial extension of the higher index wave functions is expected for a quadratic confinement potential. Note that especially for the lowest

dx.doi.org/10.1021/nl401217q | Nano Lett. 2013, 13, 3571–3575

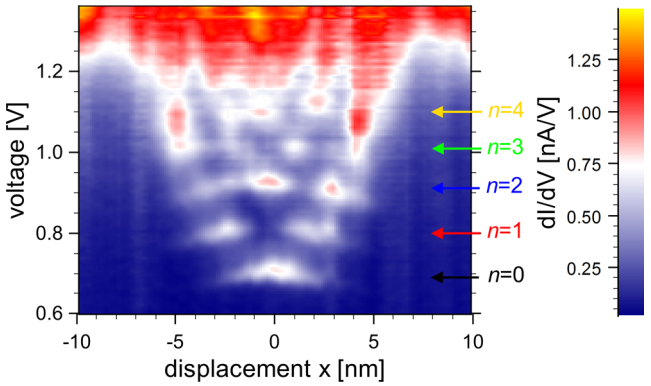

Figure 3. Differential conductivity $dI/dV(x,V)$-section along the quantum dot in [110] direction. The differential conductivity vanishes between the indicated voltages at n = 0−4.

three states, the differential conductivity practically vanishes when the bias voltage does not correspond to the eigenstate energy of the level. From this we conclude that indeed distinct wave functions are mapped. A section through the dI/dV peaks along the y-direction (Figure 3: voltage axis) was taken and from the width of the peak the energetic uncertainty of the energy quantization was estimated to be ±25 mV.

Why do the wave functions of the InAs QD under investigation reveal the characteristics of a 1D harmonic oscillator? For lens-shaped self-assembled InAs QDs embedded in a host material such as AlAs the QD potential can be separated into a z-component (growth direction) with strong confinement and large quantization energy and a radial component with weaker confinement in the x-y-basal-plane of the quantum dot.[18] Quantization effects from the confinement in the z-direction for higher quantum states are too large to be observed in the relevant bias range of our experiments. Since in our experiment the QD is cut near the diameter in the $(1\bar{1}0)$ plane only about half or less of the lens shaped QD remains and the full rotational symmetry is lost. Again the depth of the remaining QD in $[1\bar{1}0]$ direction is smaller than the diameter leading to a higher eigenstate energy of the states quantized in the $[1\bar{1}0]$ direction compared to the [110] states. Therefore, again, the higher $[1\bar{1}0]$ states are not found in the relevant bias voltage range below 1.2 V of Figure 2 and Figure 3. As a consequence the one-dimensional QD confinement along [110], which can be well approximated by a one-dimensional harmonic oscillator potential, is dominant in the relevant bias voltage range.

Note that the chosen high band gap material AlAs (band gap ∼3 eV) as a host material is particularly advantageous for the observation of these well-defined InAs QD wave functions. Despite of the large energy spacing five levels with almost constant level spacing are observed. In contrast, in GaAs (band gap ∼1.5 eV) only three levels with decreasing energy spacing have been found[10] speaking for the influence of the lower conduction band energy.

In Figure 3 for higher bias voltages above ∼1.2 V, the wave functions of level n = 5 do no longer show harmonic oscillator-like behavior. Here, a broad dI/dV distribution is observed that might be related to the superposition of wave function components from the stronger quantized QD states of the other crystal directions. A merge of the harmonic potential into the AlAs conduction band at these bias voltages is not probable since this would not agree with the observed equidistant level spacing. However, a leaking of the QD wave functions into the quasi continuum of the two-dimensional InAs wetting layer or into the X-band of the AlAs matrix might also occur. These effects have been reported in tunneling experiments in a similar energy range.[16]

So far we have shown that the experimental data of the InAs wave function distribution in space and energy qualitatively agrees with the predictions of a 1D harmonic oscillator model. For a more quantitative comparison with the solution of the Schrödinger equation, one needs the energy difference of the states, as well as the effective mass m^* of the electron in the quantum dot. Unfortunately, both values are not exactly known. Because of the influence of the tip-induced band bending (TIBB), the measured voltage difference of 100 mV is not necessarily the exact energy difference of the states. The effective mass for InAs bulk material is known, but the small, strained quantum dot does not necessarily show a bulklike behavior. Furthermore the effective electron mass in this small volume will be influenced by the surrounding material.[18]

Nonetheless, the ideal mechanical harmonic oscillator can be fully described by introducing a characteristic length X_0

$$X_0 = \sqrt{\frac{\hbar}{\omega m^*}} \tag{1}$$

with the frequency ω, Planck's constant $\hbar$, and the electron effective mass m^*. By this, both unknown parameters, m^* and the energy spacing, are reduced to the parameter X_0 and the solutions of the harmonic oscillator potential the wave functions Ψ can be calculated[19]

$$\psi_n = (2^n n! \sqrt{\pi} X_0)^{-1/2} \exp\left(-\frac{1}{2}\left(\frac{x}{X_0}\right)^2\right) H_n\left(\frac{X}{X_0}\right) \tag{2}$$

Here n is a non-negative integer, labeling the different states, and H_n are the Hermite polynomials. The corresponding eigenenergies are

$$E_n = \hbar\omega\left(n + \frac{1}{2}\right) \quad \text{for} \quad n \geq 0 \tag{3}$$

In Figure 4, cross sections of the measured differential conductivity $dI/dV(x,y)$-maps, taken along the line indicated by

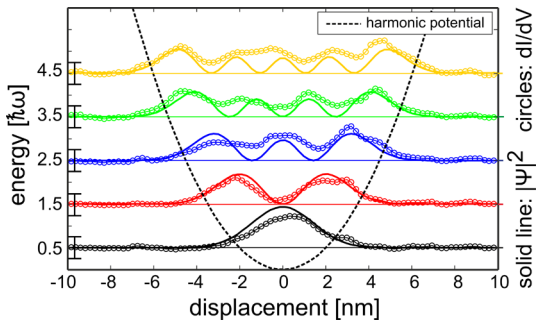

Figure 4. The circular data points show $dI/dV(x)$-sections taken along a vertical line through the quantum dot states in the $dI/dV(x,y)$-maps in Figure 2. The data points are fitted to the eigenfunctions of the one-dimensional harmonic oscillator potential (solid lines). The fitting parameter is the characteristic length, the best fit is obtained for X_0 = 2.0 nm. The potential is drawn as a black dotted line. The energy is plotted in the dimension of $\hbar\omega$; the wave functions and the differential conductivity are plotted in arbitrary units.

dx.doi.org/10.1021/nl401217q | Nano Lett. 2013, 13, 3571−3575

the arrows in Figure 2b, are shown (circles). They are compared to the solutions of the first five wave functions (n = 0−4) of the 1D harmonic oscillator potential (solid line). From the measured data, a dI/dV offset is removed, such that in the area of −10 to −8 and +8 to +10 nm the dI/dV signal is zero. The dI/d$V(x)$ sections are multiplied with a scaling factor to coincide the amplitude of the experimental data with the calculated wave functions. The scaling factor is the same for all five data sections. The characteristic length X_0 is used as fitting parameter and is again the same for all five wave functions. The fitting is done by minimizing the difference between the experimental data and the calculated wave functions for all five wave functions simultaneously. The best fit is obtained for a characteristic length of X_0 = 2.0 nm. The corresponding harmonic potential is illustrated by the dashed line in Figure 4. The energy is plotted in units of $\hbar\omega$ (left vertical axis). The energetic uncertainty of the measurement is indicated by the error bars on the left side of the image. Despite of the simple textbook model, a remarkable agreement with the experimental data is found especially for the three lowest states. The obtained characteristic length of X_0 = 2.0 nm is smaller than the value of X_0 = 5.3 nm observed in capacitance spectroscopy experiment on InAs QDs in GaAs[18] confirming the stronger confinement of InAs/AlAs QDs.

When neglecting the effect of TIBB, the measured energetic difference of the states is 100 meV. Hence according to eq 1 an effective mass of m^* = 0.19m_0 can be derived. To estimate the effect of TIBB on the energetic spacing and hence on m^* the potential landscape of the system was calculated numerically using a commercial finite element solver.[20] The geometry of the heterostructure, the tip, and its corresponding dielectric constants were included. For different applied voltages, the Poisson equation was calculated self-consistently[21] and a reduction of about 20% for the energetic difference due to TIBB was extracted. Thus, a true energy spacing of 80 meV between the eigenstates is estimated. This value is comparable to the energy differences of ground and exited states derived from photoluminescence studies of InAs QDs in an AlAs matrix.[22]

The resulting effective oscillator mass including TIBB is m^* = 0.24m_0 and thus an order of magnitude larger than the conduction band edge mass of bulk InAs of $m^*(\Gamma)$ = 0.026m_0.[23] This rather large difference could be related to the small QD dimensions and the resulting influence of the surrounding AlAs matrix. AlAs has higher bulk effective electron mass values of $m_l^*(X)$ = 0.97m_0 and $m_t^*(X)$ = 0.22m_0 for the longitudinal and the transversal X-band mass,[23] respectively. Hence a penetration of the wave function from the small QD into the surrounding AlAs should result in a higher effective oscillator mass. Also intermixing of AlAs from the surrounding matrix into the InAs QD could contribute to the observed increase of m^*. Additional effects that cannot be ruled out could be related to strain and to the nonparabolicity of the bands in k-space.[18]

The detailed understanding of the wave functions of self-assembled QDs gained by STS could in the future prove valuable for improving the electronic and opto-electronic properties of QD devices that are inseparably tied to the wave function properties. For example, in resonant tunneling diodes the onset voltage of the tunneling current depends strongly on the electronic ground state energy levels of the QDs.[15] Furthermore, in QD lasers,[24] IR emitters,[25] or photodetectors,[26] the operation wavelength is determined by the energy level separation. Although the QD size and band gap are important also, the matrix material can strongly affect the electronic properties. In practice, this could be used, for example, to shift the photoluminescence emission energy of InAs QDs by alloying a specific amount of Al into the GaAs host matrix. Note that in many kind of QD devices QD ensembles are present and inhomogeneous energy broadening, for example, due to size stray and material intermixing has to be considered. However, especially for single-QD devices like single-photon emitters[27] the detailed knowledge of specific wave function properties could significantly improve device performance. Note that despite the good agreement of the data and the one-dimensional oscillator model, one has to keep in mind the limits of this simple model. Here, for larger QDs[14] and narrow gap matrix materials stronger deviations can be expected.[10] Furthermore, if the spatial QD extensions in all three dimensions are comparable the simple one-dimensional model will not hold and more complex wave functions will form.[2]

In conclusion, the wave functions of an InAs quantum dot embedded in an AlAs matrix of a resonant-tunneling diode were resolved in space and energy by cross-sectional scanning tunneling spectroscopy. The differential conductivity maps reveal the textbook-like characteristics of a one-dimensional quantum-mechanical harmonic oscillator with five equidistant electronic energy levels. The oscillator is characterized by an effective length of 2.0 nm, an energy level spacing of 80 meV, and an effective oscillator mass of 0.24m_0. This effective mass is much larger than the effective electron mass of bulk InAs that is attributed to the influence of the surrounding AlAs matrix. This strong influence of the host material on the quantum mechanical properties of embedded self-assembled QDs must be taken into account when tailoring the QD properties for specific device applications.

AUTHOR INFORMATION

Notes

The authors declare no competing financial interest.

ACKNOWLEDGMENTS

K.P and H.W.S acknowledge funding by DFG also within SPP1285 and support of MBE sample growth by H. Marx. M.W, K.T, H.P, and R.G.U acknowledge funding by DFG-SPP 1285.

REFERENCES

(1) Marcinkevicius, S. Self-Assembled Quantum Dots. In *Lecture Notes in Nanoscale Science and Technology*; Wang, Z., Ed.; Springer: New York, 2008; Vol. *1*, pp 129−163.

(2) Maltezopoulos, T.; Bolz, A.; Meyer, C.; Heyn, C.; Hansen, W.; Morgenstern, M.; Wiesendanger, R. *Phys. Rev. Lett.* **2003**, *91*, 196804.

(3) Patanè, A.; Hill, R. J. A.; Eaves, L.; Main, P. C.; Henini, M.; Zambrano, M. L.; Levin, A.; Mori, N.; Hamaguchi, C.; Dubrovskii, Y. V.; Vdovin, E. E.; Austing, D. G.; Tarucha, S.; Hill, G. *Phys. Rev. B* **2002**, *65*, 165308.

(4) Patanè, A.; Mori, N.; Makarovsky, O.; Eaves, L.; Zambrano, M. L.; Arce, J. C.; Dickinson, L.; Maude, D. K. *Phys. Rev. Lett.* **2010**, *105*, 236804.

(5) Wibbelhoff, O. S.; Lorke, A.; Reuter, D.; Wieck, A. D. *Appl. Phys. Lett.* **2005**, *86* (9), 092104.

(6) Bester, G.; Reuter, D.; He, L.; Zunger, A.; Kailuweit, P.; Wieck, A. D.; Zeitler, U.; Maan, J. C.; Wibbelhoff, O.; Lorke, A. *Phys. Rev. B* **2007**, *76*, 075338.

(7) Bruls, D. M.; Vugs, J. W. A. M.; Koenraad, P. M.; Salemink, H. W. M.; Wolter, J. H.; Hopkinson, M.; Skolnick, M. S.; Long, F.; Gill, S. P. A. *Appl. Phys. Lett.* **2002**, *81* (9), 1708−1710.
(8) Blokland, J. H.; Bozkurt, M.; Ulloa, J. M.; Reuter, D.; Wieck, A. D.; Koenraad, P. M.; Christianen, P. C. M.; Maan, J. C. *Appl. Phys. Lett.* **2009**, *94* (2), 023107.
(9) Grandidier, B.; Niquet, Y. M.; Legrand, B.; Nys, J. P.; Priester, C.; Stiévenard, D.; Gérard, J. M.; Thierry-Mieg, V. *Phys. Rev. Lett.* **2000**, *85* (5), 1068−1071.
(10) Urbieta, A.; Grandidier, B.; Nys, J. P.; Deresmes, D.; Stiévenard, D.; Lema, A.; Patriarche, G.; Niquet, Y. M. *Phys. Rev. B* **2008**, *77*, 155313.
(11) Girard, J.; Lemaître, A.; Miard, A.; David, C.; Wang, Z. Z. *J. Vac. Sci. Technol., B* **2009**, *27*, 891.
(12) Gaan, S.; He, G.; Feenstra, R. M.; Walker, J.; Towe, E. *Appl. Phys. Lett.* **2010**, *97* (12), 123110.
(13) Fain, B.; Girard, J.; Elvira, D.; David, C.; Beaudoin, G.; Beveratos, A.; Robert-Philip, I.; Sagnes, I.; Wang, Z. *Appl. Phys. Lett.* **2010**, *97*, 171903.
(14) Fain, B.; Robert-Philip, I.; Beveratos, A.; David, C.; Wang, Z. Z.; Sagnes, I.; Girard, J. C. *Phys. Rev. Lett.* **2012**, *108*, 126808.
(15) Hapke-Wurst, I.; Zeitler, U.; Keyser, U. F.; Haug, R. J.; Pierz, K.; Ma, Z. *Appl. Phys. Lett.* **2003**, *82* (8), 1209−1211.
(16) Hapke-Wurst, I.; Zeitler, U.; Schumacher, H. W.; Haug, R. J.; Pierz, K.; Ahlers, F. J. *Semicond. Sci. Technol.* **1999**, *14* (11), L41.
(17) Loth, S.; Wenderoth, M.; Ulbrich, R. G.; Malzer, S.; Dohler, G. H. *Phys. Rev. B* **2007**, *76* (23), 235318.
(18) Miller, B. T.; Hansen, W.; Manus, S.; Luyken, R. J.; Lorke, A.; Kotthaus, J. P.; Huant, S.; Medeiros-Ribeiro, G.; Petroff, P. M. *Phys. Rev. B* **1997**, *56*, 6764−6769.
(19) Schwabl, F. *Quantenmechanik*, 6th ed.; Springer-Verlag: New York, 2002.
(20) *COMSOL Multiphysics*. www.comsol.com (accessed July, 6, 2013).
(21) Teichmann, K. *Scanning tunneling spectroscopy of space charge regions in semiconductors: From single donor to heterostructure systems*. Ph.D. thesis, Georg-August-Universität, Göttingen, 2012.
(22) Pierz, K.; Miglo, A.; Hinze, P.; Ahlers, F.; Ade, G.; Hapke-Wurst, I.; Zeitler, U.; Haug, R. *Phys. Status Solidi B* **2001**, *224* (1), 119−122.
(23) Vurgaftman, I.; Meyer, J. R.; Ram-Mohan, L. R. *J. Appl. Phys.* **2001**, *89*, 5815.
(24) Liu, H.; Wang, T.; Jiang, Q.; Hogg, R.; Tutu, F.; Pozzi, F.; Seeds, A. *Nat. Photonics* **2011**, *5*, 416.
(25) Wasserman, D.; Gmachl, C.; Lyon, S. A.; Shane, E. A. *Appl. Phys. Lett.* **2006**, *88*, 191118.
(26) Chang, C. C.; Sharma, Y. D.; Kim, Y. S.; Bur, J. A.; Shenoi, R. V.; Krishna, S.; Huang, D.; Lin, S. Y. *Nano Lett.* **2010**, *10*, 1704.
(27) Yuan, Z.; Kardynal, B. E.; Stevenson, R. M.; Shields, A. J.; Lobo, C. J.; Cooper, K.; Beattie, N. S.; Ritchie, D. A.; Pepper, M. *Science* **2007**, *295*, 102.